Design of unbonded precast post-tensioned piers constructed using concrete filled FRP tubes

Mohamed A. ElGawady, PhD, Dept. of Civil, Architectural & Environmental Engineering, Missouri University of Science and Technology, Rolla, MO
Haitham Dawood, MSc, Dept. of Civil and Environmental Engineering, Virginia Polytechnic Institute and State University, VA

ABSTRACT

There is a strong need to develop a bridge pier's system that can withstand high seismic events without collapse, and also that is resilient. Recently, segmental precast-post-tensioned piers show high self-centering capabilities compared to conventional reinforced concrete piers. This paper presents a seismic design procedure for self-centering precast post-tensioned bridge piers. The piers presented in this manuscript consisted of concrete filled fiber reinforced polymer (FRP) tubes. A large set of 84 piers with different design parameters were analyzed using finite element models. The backbone curve of each pier was developed and bilinearized. The idealized backbone curves were used to develop a set of empirical equations that were able to reproduce the bilinearized backbone curve of a given pier. Different performance criteria have been proposed for the system according to the intensity and the frequency of occurrence of a seismic event. The developed empirical equations were arranged in a design procedure to achieve a given performance level at a specific seismic zone.

Keywords: Finite Element Analysis, Analytical Modeling, Columns, Piers, Seismic, Fiber Reinforced Polymer

SEGMENTAL PRECAST POST-TENSIONED (SPPT) PIERS

The Kobe earthquake (Japan 1995) resulted in demolishing over 100 reinforced concrete bridge piers that reached residual drift angles in excess of 1.5%[1]. This showed the need for a bridge pier's system that not only can withstand high seismic events without collapse, but also that is resilient. Recently, segmental precast-post-tensioned (SPPT) piers show high self-centering capabilities compared to conventional reinforced concrete (RC) piers[2-6].

Fiber reinforced polymer (FRP) are widely used for bridge retrofitting. Recently, concrete filled FRP tubes (CFFT) have been used as an economical solution for durability issues of concrete bridges[7]. ElGawady and Booker[8], ElGawady et al.[9], and ElGawady and Shaalan[10] investigated the seismic behavior of SPPT columns and bents consist of precast CFFT segments stacked over each other and connected by unbonded post-tensioning tendons (Fig. 1). The segments had no reinforcement but the post-tensioning tendon and the FRP tubes.
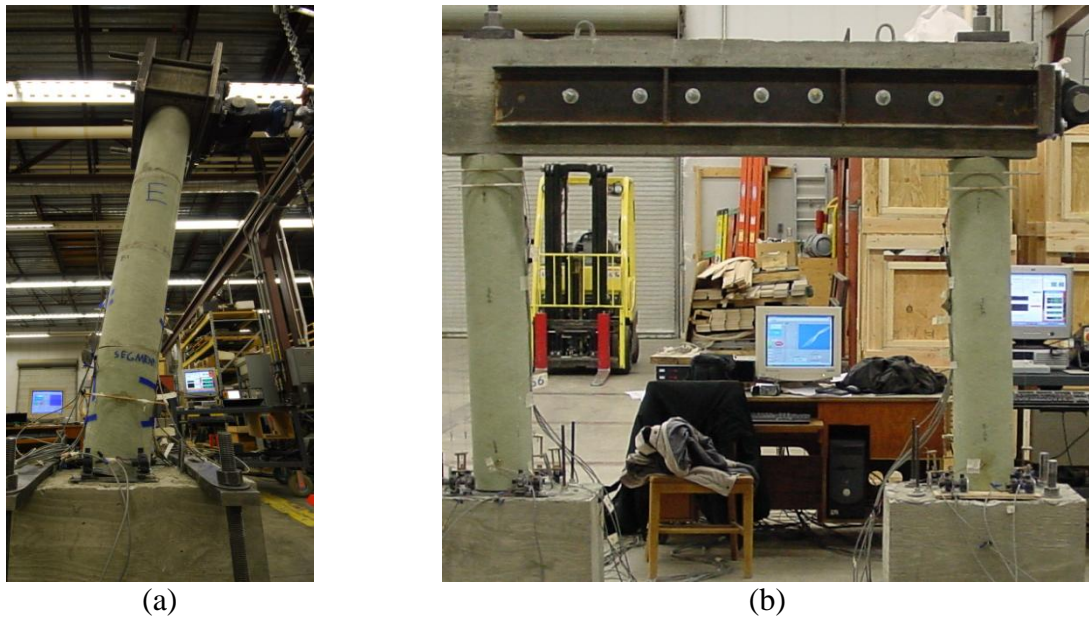

(a)   (b)

Fig. 1 Segmental column and bents during testing[8-10]

ElGawady and Shaalan[10] found that the residual displacements for a SPPT bridge bent is approximately 10% of the maximum imposed lateral displacement on that bent. The residual drift angles of the SPPT piers studied by Hewes and Priestley[4] were approximately 4% to 5% of the maximum imposed lateral displacement.

Equivalent viscous damping is an essential parameter that affects the behavior of a structural system under seismic excitations. Hewes and Priestley[4] reported an average equivalent viscous damping of approximately 5% up to a drift angle of 3% with higher values associated with low confinement due to the damage increase; then, it increased due to spalling of concrete cover of the reinforced concrete segments. Chou and Chen[2] reported that the equivalent viscous damping was 6.5% on average for SPPT piers with a minimum value that

was approximately 6%. ElGawady et al.[9] reported an average equivalent viscous damping of 5% for single segmented pier similar to those investigated in this study.

All the above mentioned experimental works showed the advantage of the SPPT system; however, there is no design procedure developed for SPPT system. This manuscript presents a design procedure for SPPT piers using empirical equations. To accomplish this target, a set of 84 piers having different design parameters were analyzed using a 3D finite element (FE) models. Nonlinear regression analyses were carried out on the results of this set of piers. The regression analysis resulted in a set of empirical design equations.

SUMMARY OF 3D FINITE ELEMENT MODEL FOR SPPT

ABAQUS/Standard[11] version 6.8-2, a general purpose finite element code, was selected as a basic platform for developing a 3D finite element (FE) model for this study. The model was presented in detail by ElGawady and Dawood[12] and verified against three different experimental studies[12-14].

In this manuscript, the SPPT system consisted of one precast segment sandwiched between foundation and superstructure. All piers in this study consisted of concrete filled glass fiber reinforced polymer (GFRP) tubes without any rebar. The system is connected by unbonded post-tensioning tendons passing through ducts made in the segments during casting. The model was built up using 3D continuum elements for concrete and fiber components and 3D beam elements for the post-tensioning tendons (Fig. 2).
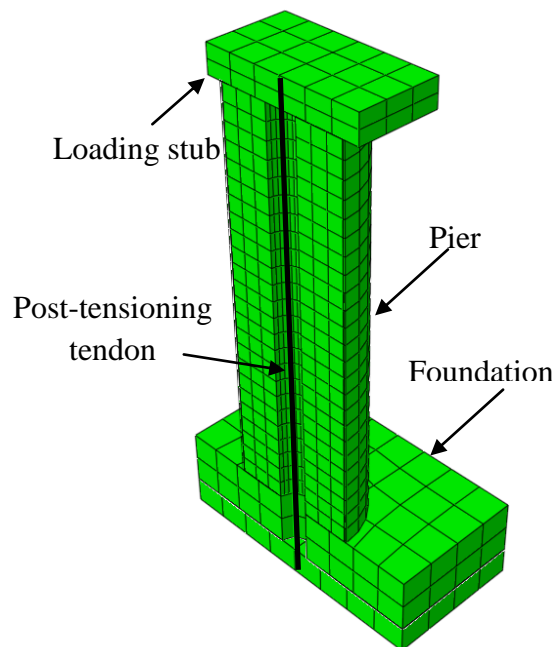

Fig. 2 FE model for a SPPT pier used in this study

The concrete damaged plasticity model[15-16] was used to model the concrete material behavior while the classic metal plasticity model was used for the tendon's material. The fiber tube was modeled as an elastic orthotropic material. The ends of the tendon were embedded in the loading stub (that represents the superstructure) and the foundation to simulate the tendon's anchorage. The tendon was subjected to a stress type initial condition to simulate its post-tensioning. By neglecting the sliding of the foundation and by assuming a rigid soil underneath the foundation, the bottom surface of the foundation was constrained in the three motional directions.

Three loading steps were used for the analysis of the models. During the first step, a post-tensioning force was applied using a stress-type initial condition to the tendons. During the second step, the gravity load was applied as a traction force applied to the top surface of the model. The third loading step consisted of a monotonic push in the lateral direction simulated by a linearly increasing lateral displacement until the failure of the model occurs and the analysis was not able to proceed any further.

Fig. 3 shows the deformed shape of a pier due to the application of the lateral loads. As shown in the figure, the pier attained its lateral deformation through opening of the interface joint at the base. The FE model successfully captured the overall behavior of the system (i.e., the backbone behavior, stress concentrations at the pier's toe and failure modes). More details about the model description, its implementation and validation procedures along with in-depth parametric studies are presented by Dawood [13].
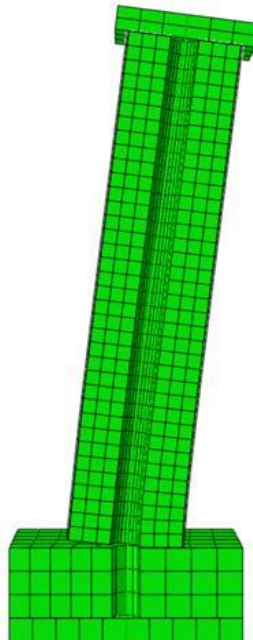

Fig. 3 Deformed shape of the pier

CURRENT STUDY DESCRIPTION

The previously described FE model was used to investigate the behavior of a large matrix of 84 piers having different design parameters, namely, height, diameter, effective post-tensioning load, and external gravity load. The values studied for each parameter are listed in Table 1. The piers were built up using plain concrete with a characteristic compressive strength (f'c) of 41.4 MPa [6000 psi] cast directly in glass fiber reinforced polymer (GFRP) confining tubes 19 mm [0.75in] thick (Table 2). The material characteristics of the tube were assumed based on commercially available GFRP materials. The wall thickness of the tubes was designed to avoid brittle shear failure under the anticipated ultimate lateral load of the piers.

Table 1: Different investigated parameters for the SPPT piers

Height	Diameter	PT	DL
1830 mm [72 in]	1220 mm [48 in]	10%	5%
3660 mm [144 in]	610 mm [24 in]	15%	7%
5490 mm [216 in]	-	20%	10%
9144 mm [360 in]	-	30%	-

Table 2: Material Properties of the GFRP tubes

Flexural Modulus Longitudinal	13790 MPa [2,000 ksi]
Tensile Strength Longitudinal	634 MPa [9.2 ksi]
Poisson's Ratio	0.35

The investigated piers have heights ranging from 1830mm [72 in] to 9144mm [360 in] and cross sectional diameter of either 1220 mm [48 in] or 610 mm [24 in]. This resulted in piers having aspect ratios of 3 to 15. The stress on the concrete induced by the gravity load normalized by its confined concrete ultimate strength f'$_{cc}$ (DL) ranged from 5% to 10%. While, the stress on the concrete induced by the post-tensioning force normalized by its f'$_{cc}$ (PT) ranged from 10% to 30%, where f'$_{cc}$ is the failure stress of the confined concrete.
Throughout this study, Samaan et al.'s[17] model was used for developing the stress-strain behavior of concrete confined by GFRP. Fig. 4 shows the developed stress strain curves for the concrete of piers with different diameters. As shown in the figure, although the GFRP and concrete were identical in both cases, the confining effect increased as the diameter of the cross section decreased. The concrete was defined using a density of 2214 kg/m^3 [0.08 lb/in^3], Young's modulus of 25,414MPa [3686 ksi] and a Poisson's ratio of 0.2.

The post-tensioning tendon used in the investigation resulted in a reinforcement ratio of 2.00% and 2.35% for piers having cross sectional diameters of 1220 mm [48 in] and 610 mm [24 in], respectively. These diameters were selected such that the post-tensioning stress in the tendons were 20% (25%), 30% (38%), 40% (51%) and 60% (76%) of their ultimate (yield) strength. The axial stresses in the piers cross sections due to these applied post-tensioning forces (PT) were 10%, 15%, 20% and 30% of f'$_{cc}$, respectively. The post-tensioning tendon was defined with a Young's modulus of 204,774 MPa [29,700ksi], Poisson's ratio of 0.3, yield stress of 874 MPa [126.8 ksi] and ultimate stress of 1110 MPa [160.9 ksi].
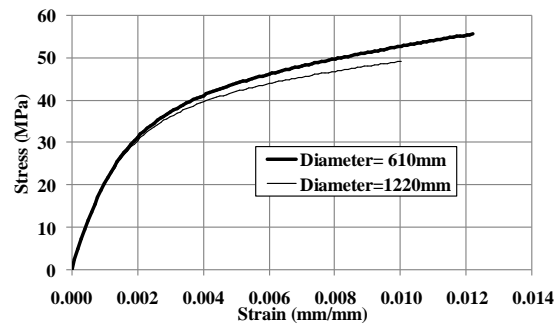
Fig. 4: Compressive stress strain relationship for concrete encased in GFRP tubes

PERFORMANCE LEVELS

The performance-based seismic design of a structure necessitates specifying performance criteria for each seismic hazard level. Two performance levels, namely collapse-prevention and serviceability, were proposed[18-19] for the design of unbonded post-tensioned piers and masonry walls. However, there is no consensus on the different performance levels and its criteria for unbonded post-tensioned structural elements. For the SPPT system investigated in this study, the following performance levels were adopted.

Performance Criteria for Serviceability Level of SPPT Piers

The serviceability performance point is associated with the smallest among: a) drift angle when the concrete reaches its theoretical ultimate confined strain (ε_{cu}); b) drift angle at which the stress in the tendon reaches 90% of its yield stress; c) drift angle corresponding to 70% of the pier's ultimate drift angle; and d) drift angle of 2%. The drift angle is defined as the ratio between the measured lateral displacement at the point of load application and the height of this point of load application above the pier's foundation.

Criterion 'a' was chosen to insure that no toe crushing will occur, similar criterion was adopted[19] for rocking masonry walls. Currently, the available models for predicting the stress-strain behavior of confined concrete are quite conservative in predicting the ultimate strain[6, 17, 20-22]. Hence, a rocking pier should be able to resist lateral loads well beyond those causing the confined concrete to reach its theoretical ultimate strains. In addition, experimental work showed that rocking piers suffered minimal, easy repairable, damage with minimal residual crack widths when they were subjected to lateral loads causing the confined concrete, at their toes, to reach its theoretical ultimate strain.

Criterion 'b' was chosen as a fraction of the yielding stress of the tendon to give a margin of safety against yielding. Wight et al.[19] adopted similar criterion for rocking masonry walls. Kurama[23] and Kwan and Billington[18] used 100% of f_y as a criterion for the serviceability performance level. However, yielding of tendons leads to loss in the applied post-tensioning forces, stiffness degradation, and reduction in the self-centering capability of the SPPT

system. Hence, the authors of this manuscript believe in having a margin of safety against yielding of the post-tensioning tendons.

Criterion 'c' was adopted by Kwan and Billington[18] to provide the piers with a sufficient margin of safety against brittle failure. Criterion 'd' was proposed also to ensure a sufficient margin of safety against brittle failure and to ensure minimal residual drift angle.

For rocking structures, criteria 'a' and 'b' may occur just before or after the collapse-prevention performance level. This indicated the importance of criteria 'c' and 'd'.

Performance Criteria for the Collapse-Prevention Level

The collapse-prevention performance point is associated with the smallest drift angle among: a) drift angle at which the post-tensioning tendons yield; b) drift angle level of 4.5%; and c) drift angle that cause a residual drift angle of 1.0%.

Criterion 'a' was chosen to avoid tendons yielding as discussed before[18, 23]. Criterion 'b' was adopted from Priestley et al. [24] who recommended this drift level for collapse prevention in bridges. Criterion 'c' was adopted from Kwan and Billington[18]. Based on available experimental data on SPPT piers similar to those examined in this manuscript, a residual displacement of 10% of the imposed lateral displacement would be appropriate. Hence, criterion 'b' will always govern over criterion 'c'. This assumption would be revised in the future when more experimental data become available.

STUDY PROCEDURE

This study, according to the authors' best knowledge, represents the first attempt to develop a performance-based design procedure for SPPT. Hence, more deliberation and validation against dynamic tests are required. To accomplish this study, the following steps were carried out: a) the serviceability and collapse-prevention performance levels were determined using the criteria discussed before; b) the backbone curves obtained from the results of the FE models of the 84 piers were bilinearized following FEMA 356, in this case the performance displacement for serviceability and collapse-prevention were used as Δ_u in the FEMA procedure (Fig. 4) (i.e., for each pier two bilinearized backbone curves were prepared); c) each parameter in the bilinear backbone curve (i.e. K_e, Δ_y, F_y, Δ_u, F_u and α (Fig. 4)) was studied separately and nonlinear regression analyses were carried out to develop empirical equations for the prediction of each parameter; d) empirical equations for predicting the post-tensioning stresses in the tendon, at different drift levels, were derived; e) a simplified systematic procedure was derived for the design of SPPT pier system using the developed empirical equations. Once the empirical equations were developed, the errors in predicting the parameters corresponding to the bilinear system were calculated using Eq. 1.

Error in calculating parameter A (%) = $\frac{A_{from\ the\ empirical\ equation} - A_{from\ the\ bilinear\ approximation}}{A_{from\ the\ bilinear\ approximation}}$

%   (1)

Idealized Backbone Curves at Collapse-Prevention And Serviceability Performance Levels

Effective stiffness (K$_{CP-e}$ and K$_{S-e}$)

The nonlinear regression analyses of the data of the 84 piers showed that the effective stiffness is a function of (EI/H); where, E: is the modulus of elasticity of the pier's concrete (kN/mm^2); I: is the moment of inertia of the pier's cross section (mm^4); and H is the height of the pier (mm). The effective stiffness was found to be inversely proportional to PT. Eq. 2 was found to best predict the effective stiffness for both, the collapse prevention (K$_{CP-e}$) and serviceability (K$_{S-e}$) performance levels.

$$K_{CP-e}\ (kN/mm) = K_{S-e}\ (kN/mm) = \frac{1.82}{PT^{0.3}}\frac{3EI}{H^3}$$ (2)

Yield loads (F$_{CP-y}$ and F$_{S-y}$)

For a rocking structure, the apparent yielding of the structure is different from yielding of the unbonded tendon and occurs well before the tendons' yield[18]. In this manuscript, the yield load will be used to refer to the apparent yielding of the structure and it was defined as the lateral load at which the stiffness of the pier reduces abruptly by a factor α (Fig. 5). Fig. 6 shows the relationship between the design parameters of the piers vs. the yield loads of the piers (kN) corresponding to collapse prevention limit state (F$_{CP-y}$) and serviceability limit state (F$_{S-y}$). The load combination is represented by the horizontal axis and is defined as two percentages separated by a dash; the first (left, PT) is the stress on the concrete induced by the post-tensioning; and the second (right, DL) is the stress on the concrete induced by the gravity load. Both were normalized by f'$_{cc}$. In the figure, piers with the same dimensions are assigned a specific marker type and a code for each dimension is shown under the figure (e.g., H5490-D0610 is a pier with a height of 5490 mm and a diameter of 610 mm).

Fig. 6 shows that F$_{CP-y}$ and F$_{S-y}$ are directly proportional to the value of the combination of loads acting on a given pier. For piers with the same diameter, increasing the height decreases F$_{CP-y}$ and F$_{S-y}$. On the other hand, for piers with the same height, increasing the diameter increases F$_{CP-y}$ and F$_{S-y}$. Based on the previously mentioned observations, Eqs. 3 and 4 were developed through nonlinear regression analyses.

$$F_{CP-y}\ (kN) = \frac{D^{2.8}PT^{0.4}DL^{0.2}}{406\ H}$$ (3)

$$F_{S-y}\ (kN) = \frac{D^{2.8}PT^{0.4}DL^{0.2}}{480\ H}$$ (4)

Where D is the diameter of the pier (mm).

Fig. 5 Backbone and idealized curves

(a)   (b)

▲ H1830-D0610 ◇ H5490-D1220 ▽ H9144-D1220
○ H3660-D1220 ◆ H5490-D0610 ▼ H9144-D0610
● H3660-D0610
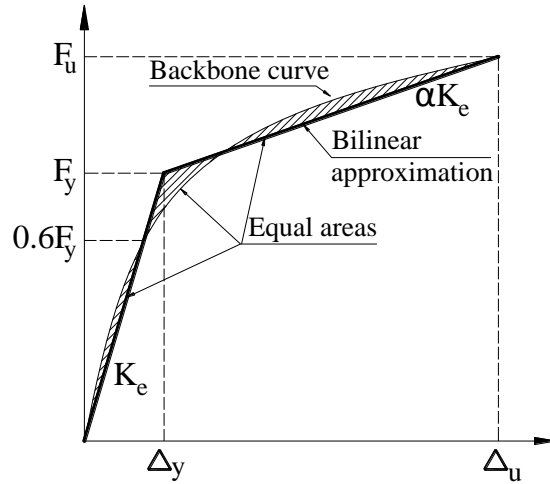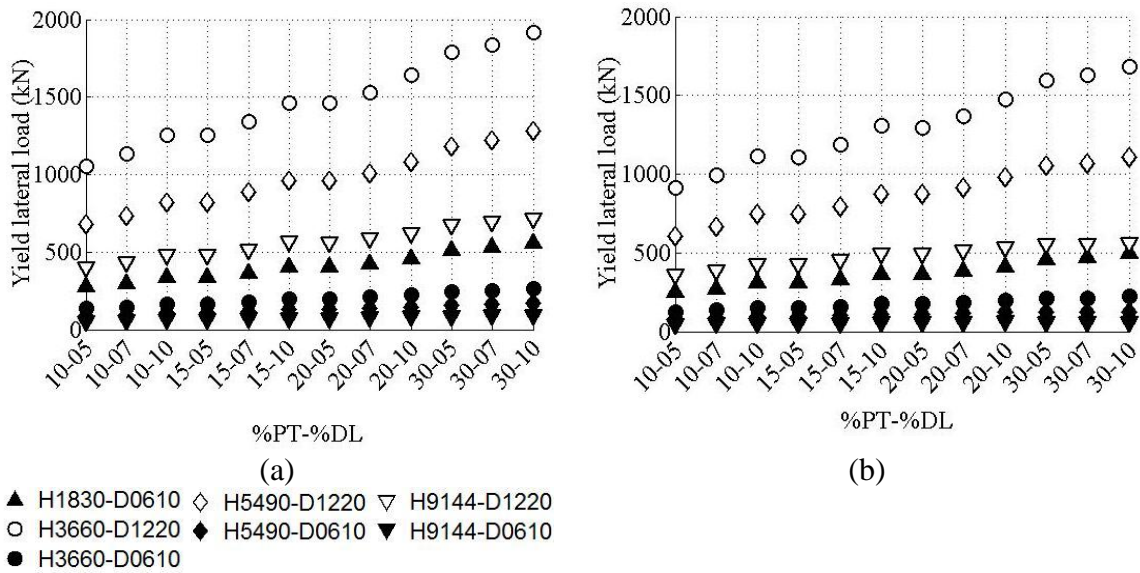
Fig. 6 The yield load associated with each specific pier for a) collapse-prevention
performance level; and b) serviceability performance level

Displacements corresponding to yield loads ($\Delta_{CP\text{-}y}$ and $\Delta_{S\text{-}y}$)

The yield displacements for collapse-prevention ($\Delta_{CP\text{-}y}$) and serviceability ($\Delta_{S\text{-}y}$) performance levels were calculated using Eqs. 5 and 6, respectively.

$$\Delta_{CP\text{-}y} \text{ (mm)} = \frac{F_{CP-y}}{K_{CP-e}} \tag{5}$$

$$\Delta_{S\text{-}y}\ (mm) = \frac{F_{S-y}}{K_{S-e}} \tag{6}$$

Performance displacements ($\Delta_{CP\text{-}P}$ and $\Delta_{S\text{-}P}$)

The collapse-prevention performance displacement ($\Delta_{cp\text{-}p}$) is the lateral displacement that fulfills all the collapse-prevention performance criteria discussed earlier in this manuscript. The prevailing performance objective in all the 84 piers analyzed in this manuscript was the 4.5% of lateral drift angle (criterion b). As a result, the collapse-prevention performance point can be calculated using Eq. 7.

$$\Delta_{cp\text{-}p}\ (mm) = 4.5\%\ H \tag{7}$$

The serviceability performance displacement ($\Delta_{S\text{-}P}$) is the lateral displacement that fulfills all the serviceability performance criteria discussed earlier in this manuscript. Criteria "d" dominated the performance of all the 84 piers; hence, Eq. 8 can be used to calculate the the performance displacement at the serviceability performance level.

$$\Delta_{S\text{-}P}\ (mm) = 2.0\%\ H \tag{8}$$

Performance loads ($F_{CP\text{-}P}$ and $F_{S\text{-}P}$)

The performance loads are the lateral loads corresponding to $\Delta_{CP\text{-}P}$ and $\Delta_{S\text{-}P}$ for the collapse-prevention ($F_{CP\text{-}P}$) and serviceability ($F_{S\text{-}P}$) performance levels, respectively. Fig. 7 shows the performance loads for the 84 specimens at serviceability and collapse prevention. The figure shows that the performance loads ($F_{cp\text{-}p}$ & $F_{S\text{-}p}$) for each pier analyzed in this manuscript. The figure shows that the performance loads like the yield loads, are directly proportional to the load combination imposed on the pier as well as the pier's diameter. Also, it is inversely proportional to the pier's height. From the nonlinear regression analyses, Eqs. 9 and 10 were derived for predicting the collapse-prevention and the serviceability performance loads, respectively.

$$F_{cp\text{-}p}\ (kN) = \frac{D^{3.0}PT^{0.2}DL^{0.1}}{37\ H^{1.3}} \tag{9}$$

$$F_{S\text{-}p}\ (kN) = \frac{D^{3.0}PT^{0.3}DL^{0.1}}{344\ H^{1.1}} \tag{10}$$

INCREASES IN THE POST-TENSIONING FORCE WITH INCREASING THE APPLIED LATERAL DRIFT ANGLE

Finding an empirical correlation between the lateral displacement and the increase in the post-tensioning stresses in the tendons of SPPT piers is essential for designing the tendon's cross sectional area. Fig. 8 shows the increase in the post-tensioning stress normalized by its

initial value versus the lateral drift angle. The topmost curve represents a loading combination of 10% from PT and 5% from DL and the curves below represent 10%PT-7%DL, 10%PT-10%DL, 15%PT-5%DL, 15%PT-7%DL, 15%PT-10%DL, 20%PT-5%DL, 20%PT-7%DL, 20%PT-10%DL, 30%PT-5%DL, 30%PT-7%DL, and 30%PT-10%DL .
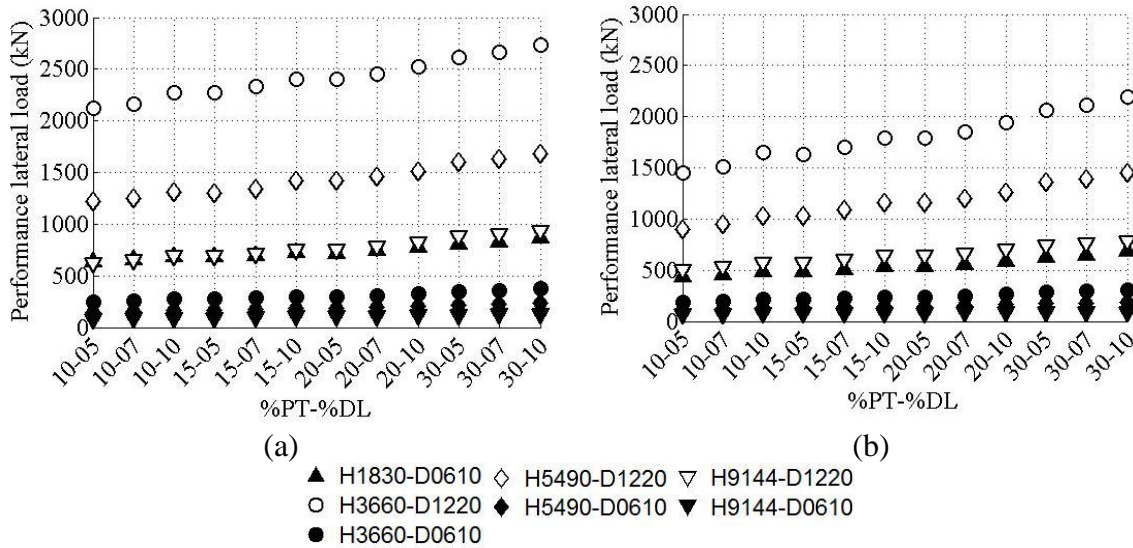

Fig. 7 The performance load associated with each specific pier: a) collapse-prevention, and b) serviceability performance levels

For high vertical load combinations, at small lateral displacements, there were reductions in the post-tensioning stresses. Beyond such displacements, the post-tensioning stresses started to increase. Once the neutral axis of the bottommost surface of the pier reached the tendon's location, the tendon started to stretch and the post-tensioning stresses increased approximately linearly versus increasing the applied lateral drift angle.

For piers subjected to relatively small vertical load combinations. The piers behaved more as a rigid block. For small lateral displacements, the post-tensioning force was approximately constant. Once the opening at the interface joint between the pier and the foundation reached the location of the tendon the post-tensioning force increased approximately linear with increasing the lateral displacement.

The different graphs presented in Fig. 8, shows that the rate of stress increase is directly proportional to the stress induced by the post-tensioning stress on the concrete. On the other hand, the stress induced on the concrete by the applied gravity load does not seem to significantly affect that slope. For piers with the same height, those with smaller diameters have much milder rate of increase of the post-tensioning stress. For piers with the same diameter, increasing the height decreases the post-tensioning stress rate of increase. Upon these observations, a nonlinear regression analysis was carried out and resulted in Eq. 11 that represents the stress in the post-tensioning tendons as a function of lateral drift angles.
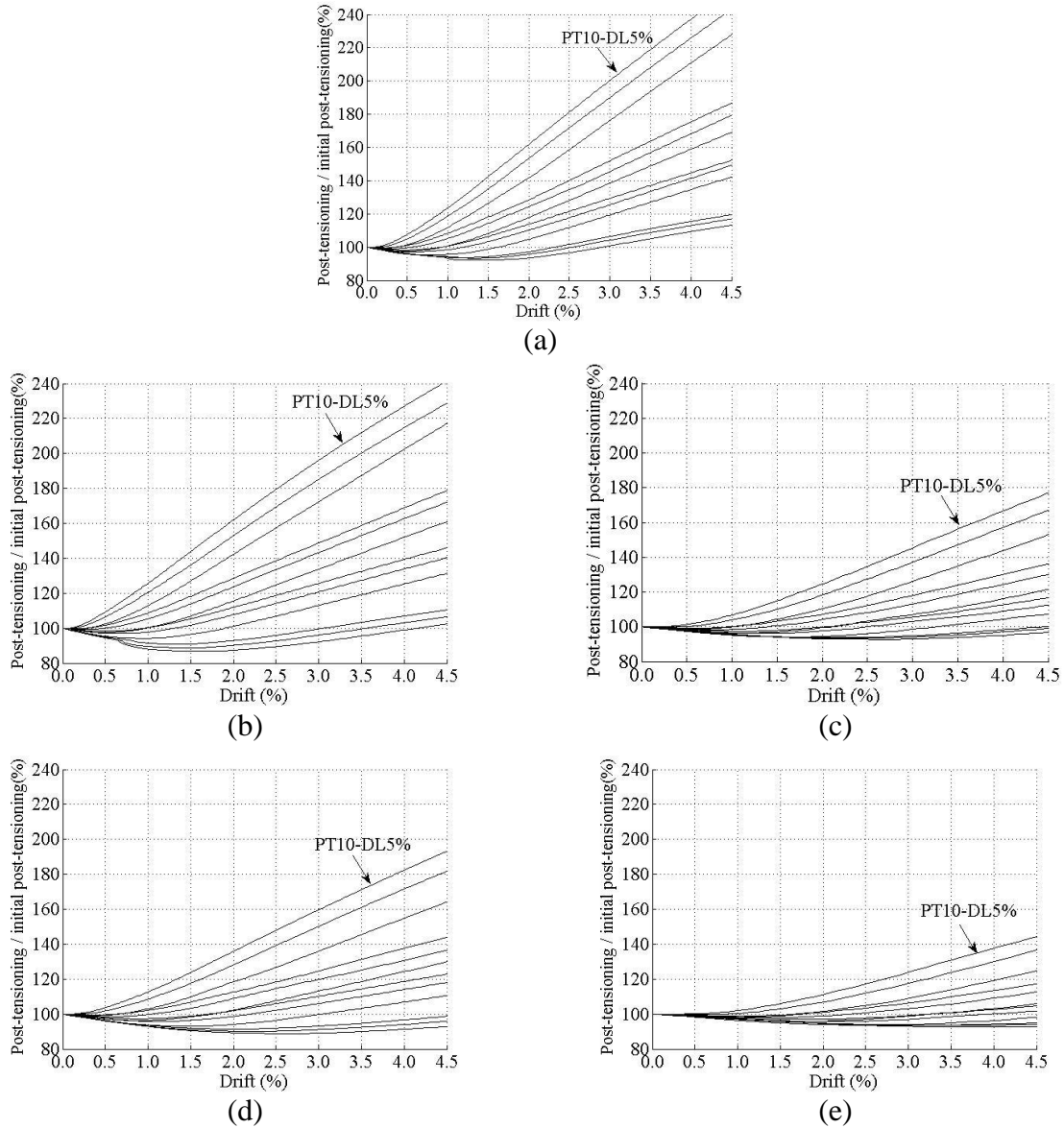
Figure 8: The relationship between the lateral drift angle (%) vs. the stress in the post-tensioning tendons normalized by its initial stress for piers; a) H1830-D0610; b) H3660-D1220; c) H3660-D0610; d) H5490-D1220; and e)H5490-D0610

$$\sigma_{PT} = \begin{cases} \sigma_i & : \delta \leq \delta_0 \\ \sigma_i \left[1 + \frac{10^2 D^{0.78}}{PT^{1.4} H} (\delta - \delta_0) \right] & : \delta > \delta_0 \end{cases} \tag{11}$$

$$\delta_0(\%) = \frac{H^{0.9} PT^{1.7} DL^{0.6}}{10^8 \, D^{0.9}} \tag{12}$$

Where, δ is the lateral drift angle of the pier (%); σ_{PT} is the final stress in the post-tensioning tendon at a lateral drift angle δ; σ_i is the effective post-tensioning stress in the tendon before

subjecting the pier to lateral loading; δ_0 is the lateral drift angle (%) at which the post-tensioning stress in the tendon starts to increase (Eq. 12).

DESIGN PROCEDURE

The proposed design procedure for the SPPT piers can be summarized in the following steps:

1) Two uniform hazard acceleration spectra (period vs. spectral acceleration) are obtained according to the location of the bridge. In this context, a constant 5% equivalent viscous damping is assumed for all drift levels as the concrete core was externally confined with the GFRP so no concrete cover spalling would occur before the rupture of the GFRP and collapse of the system. The selection of the 5% is based on the experimental work presented in the literature review section of this manuscript.

2) The two uniform hazard spectra are then converted into uniform hazard displacement spectra (period vs. spectral displacement) using Eq.13 (e.g. Priestley et al. 2007),

$$S_d(T) = \frac{T^2}{4\pi^2} S_a(T) \tag{13}$$

Where T is the period of the structure in seconds; $S_d(T)$ is the spectral displacement at a period of T seconds; and $S_a(T)$ is the spectral acceleration at a period T.

3) Given the height of the pier, the performance lateral displacements for the two performance levels (Δ_{CP-P}) and (Δ_{S-P}) can be calculated using Eqs. 5 and 6, respectively;

4) The uniform hazard displacement spectra (step 2), along with Δ_{CP-P} and Δ_{S-P}, are used to obtain the target periods of the pier at the collapse-prevention (T_{CP-P}) and serviceability (T_{S-P}) performance levels.

5) The tributary mass acting on the pier (m) along with T_{CP-P} and T_{S-P} are used to calculate the target secant stiffnesses (Eq.14) of the pier for collapse-prevention and serviceability using the respective periods (step 4).

$$K_{CP-P} = \frac{4\pi^2 m}{T_{CP-P}^2} \tag{14-a}$$

$$K_{S-P} = \frac{4\pi^2 m}{T_{S-P}^2} \tag{14-b}$$

6) The target performance lateral loads (F^*_{CP-P}) and (F^*_{S-P}) are computed by multiplying the secant stiffness (i.e., K_{CP-P} and K_{S-P}) by its corresponding performance lateral displacement.

7) A diameter (D) for the pier should be reasonably assumed or alternatively computed using Eq.15 which is an approximate equation that gives an estimation of the diameter that is most

likely to fulfill the target performance levels. The post-tensioning stress on concrete as a percentage of f'$_{cc}$ (PT*) is then calculated using Eq. 9.

$$D \text{ (mm)} = 6.3 \, F_{CP-P}^{0.33} \, H^{0.42} / T_{CP-P} \tag{15}$$

8) PT$_{CP}$ and PT$_S$ which represent the post-tensioning stress on the concrete required to assure the pier to reach the performance lateral displacement, are computed using Eqs. 9 and 10, respectively.

9) If PT$_{CP}$ ≥ PT$_S$, the final PT equals to PT$_{CP}$. This means that the pier should reach F$_{CP-P}$ at lateral displacement of Δ$_{CP-P}$. In addition, the pier will reach F$_{S-P}$ at a lateral displacement smaller than Δ$_{S-P}$. However, if PT$_S$ ≥ PT$_{CP}$, the final PT equals to PT$_S$. This means that the pier should reach F$_{CP-P}$ at lateral displacement smaller than Δ$_{CP-P}$. In addition, the pier will reach F$_{S-P}$ at a lateral displacement of Δ$_{S-P}$.

10) The target initial stress in the post-tensioning tendons (Eq. 16) is taken as the minimum of the stress values computed using Eq. 17 and 18, where; σ$_{PT-S}$ is the initial post-tensioning stress in the tendons that will make the tendons reach 90% of their yield stress when the lateral drift angle of the pier reaches δ_{S-P}; σ$_{PT-CP}$ is the initial post-tensioning stress in the tendons that will make the tendons reach 100% of their yield stress when the lateral drift angle of the pier reaches δ_{CP-P}; σ$_y$ is the yield stress of the tendons' material; δ_0 is calculated from Eq. 12.

$$\sigma_{PT} = \text{minimum of} \begin{cases} \sigma_{PT-S} \\ \sigma_{PT-CP} \end{cases} \tag{16}$$

$$\sigma_{PT-S} = 0.9\sigma_y \left/ \left[1 + \frac{100 \, D^{0.78}}{PT^{1.4} H} \times (\delta_{S-P} - \delta_0) \right] \right. \tag{17}$$

$$\sigma_{PT-CP} = \sigma_y \left/ \left[1 + \frac{100 \, D^{0.78}}{PT^{1.4} H} \times (\delta_{CP-P} - \delta_0) \right] \right. \tag{18}$$

11) The cross sectional area of the tendon (A$_{PT}$) is calculated using Eq.19, where;

$$A_{PT} = \frac{\pi D^2 \times PT \times f'_{cu}}{400 \, \sigma_{PT}} \tag{19}$$

12) If required, F$_{CP-y}$, F$_{S-y}$, Δ$_{CP-y}$, and Δ$_{S-y}$ are computed using Eqs. 3, 4, 5, and 6, respectively.

FINDINGS AND CONCLUSIONS

This manuscript presents a design procedure for segmental precast post-tensioned concrete filled fiber reinforced polymer tubes (CFFT). The piers consisted of a single precast segment sandwiched between the foundation and the superstructure with an unbonded post-tensioning

tendon passing through ducts located in the centroid of the segment. A series of 84 piers having different design parameters were analyzed using a finite element model. Criteria for two performance levels for the SPPT pier system were proposed. A set of empirical equations, capable of predicting the bilinearized backbone curve of the piers, had been developed using the results of the FE models of 84 piers. Those empirical equations had been arranged to form a design procedure for the SPPT pier system to fulfill the two performance levels. The analyses conducted in this manuscript revealed that:

- The developed empirical equations were able to predict the bilinearized backbone curve of the SPPT piers with good accuracy.
- The yield and lateral loads at the different performance levels were found to be inversely proportional to the pier's height and directly proportional to the piers diameters, stress induced on the concrete from the post-tensioning load and the external bridge gravity load.
- Within the scope of the investigated parameters, the performance of the piers was governed by the preset lateral drift angles of 4.5% and 2.0% for collapse-prevention and serviceability performance levels, respectively, with no yielding in the tendons or crushing in the concrete.
- The developed empirical equations to predict the lateral displacement vs. change in post-tensioning stresses were able to capture the behavior of the tendons. The rate of increase in post-tensioning stress was found to be directly proportional to the diameter of the pier and inversely proportional to the pier's height and the post-tensioning stress on the concrete. On the other hand, the displacement at which the increase in post-tensioning stress start was inversely proportional to the pier's diameter and directly proportional to the pier's height, post-tensioning and serviceability axial load stress acting on the pier.

REFERENCES

1. Lee, WK and Billington, SL (2010) "Residual Displacement Prediction for Structural Concrete Columns under Earthquake Loading," ASCE J. Bridge Engineering, 15(3): 240-249.
2. Chou, C.-C., and Chen, Y.-C., (2006). "Cyclic tests of post-tensioned precast CFT segmental bridge columns with unbonded strands" J. Earthquake Engng. Struct. Dyn., 35, 159-175.
3. Chang, K. C., Loh, C. H., Chiu, H. S., Hwang, J. S., Cheng, C. B., and Wang, J. C. (2002). "Seismic behavior of precast segmental bridge columns and design methodology for applications in Taiwan", Taiwan Area National Expressway Engineering Bureau, Taipei, Taiwan in Chinese.
4. Hewes, J. T., and Priestley N. (2002). "Seismic design and performance of precast concrete segmental bridge columns." Report No. SSRP-2001/25, Univ. of California at San Diego.
5. Ichikawa, S., Zhang, R., Sasaki, T., Kawashima, K., ElGawady, M., Matsuzaki, H., and Yamanobe, S., 2012. "Seismic performance of UFC segmental columns" J. of Japan Society of Civil Engineering A1 (In-Japanese)

6. Ichikawa, S., Nakamura, K., Matsuzaki, H., ElGawady, M., Kanamitsu, Y., Yamanobe, S., and Kawashima, K., 2013 (Accepted). "Enhancement of the seismic performance of bridge columns using ultra high strength fiber reinforced concrete segments"

7. Fam, A. Z., and Rizkalla, S. H., (2001), "Confinement model for axially loaded concrete confined by circular fiber-reinforced polymer tubes" ACI Str. J., 98 (4), 451-461.

8. ElGawady, M. A., and Booker, A. J., 2009. "Static cyclic response of concrete filled FRP tubes", 9th International Symposium on Fiber Reinforced Polymer Reinforcement for Concrete Structures. Sydney, Australia, July 13-15.

9. ElGawady, M. A., Booker, A. J., and Dawood, H., 2010. "Seismic behavior of posttensioned concrete-filled fiber tubes", J. Composite for Const., ASCE, 14(5), pp. 616-628.

10. ElGawady, M. A., and Sha'lan, A., 2011. "Seismic behavior of self-centering precast segmental bridge bents", J. Bridge Engineering, ASCE, 16(3), 328-339.

11. ABAQUS Software and Documentation, Version 6.8-2. © Dassault Systèmes, SIMULIA, 2008.

12. ElGawady, M. A. and Dawood, H. 2012. "Finite element analysis of self-centering bridge piers", Engineering Structures, 38, pp. 142-152

13. Dawood, H. M., "Seismic Behavior and Design of Segmental Precast Post-tensioned Concrete Piers", M.S. thesis, Washington State University, Washington, 2010

14. Dawood, H., ElGawady, M. A., and Hewes, J. 2012. "Behavior of Segmental Precast Post-Tensioned Bridge Piers under Lateral Loads", J. Bridge Engineering, ASCE, 17(5), 735-746

15. Lee, J., and G. L. Fenves, (1998) "Plastic-Damage Model for Cyclic Loading of Concrete Structures," Journal of Engineering Mechanics, vol. 124, no.8, pp. 892–900.

16. Lubliner, J., J. Oliver, S. Oller, and E. Oñate, (1989) "A Plastic-Damage Model for Concrete," International Journal of Solids and Structures, vol. 25, pp. 299–329.

17. Samaan, M., Mirmiran, A., and Shahawy, M. (1998). ''Model of concrete confined by fiber composite.'' J. Struct. Eng., 124(9), 1025–1031.

18. Kwan,W.-P., and Billington, S. L. (2003). ''Unbonded posttensioned concrete bridge piers. I: Monotonic and cyclic analyses.'' J. Bridge Eng.,8(2), 92–101.

19. Wight, G. D., Kowalsky, M. J., and Ingham, J. M., (2007). "Direct Displacement-Based Seismic Design of Unbonded Post-Tensioned Masonry Walls." ACI Structural Journal, V. 104, No. 5, pp. 560-569.

20. Beque, J., Patnaik, A. K., and Rizkalla, S., (2003), "Analytical models for concrete confined with FRP tubes" J. Composites for Construction, ASCE, 7(1), 31-38.

21. Mander, J. B., Priestley, M. J. N., and Park, R. (1988).''Theoretical stress-strain model for confined concrete.'' J. Struct. Eng., 114(8), 1804–1826.

22. Teng, J. G., Jiang, T., Lam, L., and Luo, Y.Z., (2009), "Refinement of a design-oriented stress strain model for FRP-Confined concrete" J. Composites for Construction, ASCE, 13(4), 269-278.

23. Kurama, Y. C. (1997). "Seismic analysis, behavior, and design of unbonded post-tensioned precast concrete walls." PhD dissertation, Dept. of Civil and Environmental Engineering, Lehigh University, Bethlehem, Pa.

24. Priestley, M.J.N., Calvi, G. M., and Kowalsky, M. J., "Displacement Based Seismic Design of Structures," IUSS Press, Pavia, Italy, 2007, 720pp.